Theoretical Study of Photoionization Processes in $Fe(C_5H_5)_2$

G. Fronzoni,* P. Colavita, M. Stener, G. De Alti, and P. Decleva

Dipartimento di Scienze Chimiche, Universita' di Trieste, Via L. Giogieri 1, I-34127 Trieste, Italy

Received: July 16, 2001

Density Functional calculations have been carried out to determine the photoionization cross section and the asymmetry parameter profiles of $Fe(C_5H_5)_2$, using an explicit treatment of the continuum wave function. An accurate numerical treatment is employed to ensure convergence of the calculated photoemission profiles without further potential approximation. All valence and carbon and metal core ionizations are investigated over a wide energy range. A very satisfactory agreement is obtained with the vast experimental data available for this molecule, indicating that the present LDA level of theory is generally adequate to interpret the complete photoemission spectra in organometallic compounds, with the only exception being autoionization resonances, allowing extraction of chemically relevant information from the spectra and resolution of uncertain assignments. The analysis of the calculated cross sections allows us to definitely uphold the experimental assignment of the first four outer valence ionizations and furthermore suggests that characteristic behaviors can be also recognized in the core metal cross section profiles.

1. Introduction

Ferrocene $Fe(C_5H_5)_2$ is a sandwich molecule with the iron atom symmetrically situated between two C_5H_5 rings. Since its discovery, ferrocene has been the target of many experimental and theoretical studies to develop an understanding of the electronic structure of organometallic compounds. Photoelectron spectroscopy (PES) is a very powerful tool for investigating electronic states and checking various features of the bonding interaction between metal and ligands. Consequently, a great deal of experimental and theoretical work has been devoted to the photoelectron spectrum of ferrocene, both as concerns the analysis of the ionization energy data[1−3] and the photoelectron dynamics.[4−5] The PE spectrum has been long debated and a large number of MO calculations with different degrees of sophistication have been performed[6−10] to explain the spectral features observed in the high-resolution He(I) and He(II) experimental spectra[3]. The results often appear controversial, and the assignment of the spectrum remains not completely definite for the first low ionizations. Four primary ionization processes give rise to two well-resolved bands (A′ and A″ in ref 3), which fall in the energy region below 12 eV and are associated with E_2', A_1', E_1', and E_1'' ionic states (if we refer to the eclipsed conformation (D_{5h}) of the two rings, as found in the vapor phase.) Using intensity arguments, the authors[3] have assigned the first band (A′) to the two ionizations from metal levels (e_2' and a_1') and the next two peaks in the band A" to two ionizations from the ligand levels (e_1' and e_1''), so the proposed ordering of the ion states is $^2E_2' > {}^2A_1' > {}^2E_1' > {}^2E_1''$. The different theoretical approaches have not managed to reproduce the observed pattern of ionizations in a uniform and convincing way. Only ΔSCF calculations[6,9] and very recent DFT results[11] agree with this assignment. More recent measurements of relative partial photoionization cross sections and photoelectron branching ratios of the valence bands[4] give further support to the experimental attributions. The variable energy PE spectroscopy can in fact be of considerable assistance in providing further details on the localization of the molecular level from which the electrons are ionized. For transition metal compounds, significant differences between metal and ligand cross section behavior have been observed in several experimental PES studies with variable photon energy.[12,13] In particular, the partial photoionization cross section of the ligand bands are generally featurless and decrease rapidly with increasing photon energy, whereas the cross section of the metal bands are much more structured and show a slower decline. Of course, the rationalization of experimental intensity data in terms of electronic structure of the molecular system can be strongly supported by theory which enables a more confident correlation between them. Furthermore, the analysis of the theoretical partial cross section profiles allows us to assess the different contributions carried by the different dipole allowed final continuum channels, a kind of information not generally possible in an experiment.

In light of the several experimental studies with which to compare it and the uncertainties still surrounding the photoionization data of the ferrocene molecule, we have decided to calculate cross section, branching ratios and asymmetry parameter profiles of the photoelectron bands of $Fe(C_5H_5)_2$ over a wide range of photon energies. From a theoretical standpoint, this represents also an opportunity to verify the performances of the computational method employed to describe the photoelectron dynamic observables, whose description still represents a difficult task for the quantum chemistry approaches.

In the present work, the ionizations of all orbitals, from the outer valence orbitals to the core C 1s and Fe 1s, 2p and 3p orbitals have been examined. To this purpose, the recently developed B-spline One-Centre Expansion (OCE) density functional method has been employed. This computational approach is limited to a one-electron Kohn−Sham (KS) picture, but the continuum unbound wave function is explicitly considered in the framework of the Density Functional Theory (DFT), with an accurate treatment of the molecular electronic potential. The OCE method has proven to be a reliable tool for calculating photoionization cross section and asymmetry parameter profiles of both valence and core level processes of a variety of molecules.[15−17] It is important to underline that this approach

10.1021/jp012733r CCC: $20.00
Published on Web 09/26/2001

describes both the initial and the final states of the photoionization processes without appealing to the rather crude muffin-tin (MT) approximation to the molecular electronic potential. This approximation is instead employed in the Continuum Multiple Scattering Method (CMSM),[18,19] which is the more widely used computational technique for the photoionization cross section calculations of larger molecules. In particular, in the field of transition metal complexes, only quite few continuum calculations are present in the literature, mostly performed with the CMSM approach or the even more drastically simplified Gelius model.[20−23]

In this work, the LB94 exchange correlation potential[24] in the Ground State (GS) configuration (LB94-GS) is employed in the OCE method; this potential is characterized by a correct asymptotic Coulomb behavior, which improves the results for properties sensitive to spatial regions at large distance, as in the case of cross section. This has been verified by comparing the theoretical results obtained for the cross sections of several molecular systems[25−27] with the LB94-GS potential and the VWN potential[28] (with the Transition State configuration). It is important to underscore that the use of the LB94 potential in the Ground-State configuration has the advantage of allowing the use of the same Hamiltonian for all calculations, irrespective of the particular orbital ionized, with a considerable computational economy when a large number of ionic states are considered, as in the present case.

2. Theory

The present theoretical approach is based on a large scale One Centre Expansion (OCE) to obtain accurate solution for the bound and continuum orbitals of a one particle Kohn−Sham Hamiltonian, in the framework of the Density Functional Theory. We refer to ref 14 for details of the OCE- B-spline Density Functional method.

The basis is given as products of radial B-spline functions $B_i(r)$[29] and a real spherical harmonics ($Y_{l,m}{}^R$)

$$\chi_{\mathrm{ilm}} = \frac{1}{r} B_i(r) Y_{l,m}{}^R(\theta,\varphi)$$

Any given function can be expanded in angular momentum components, accordingly to

$$f(r,\vartheta,\varphi) = \sum_{l,m} R_{l,m}(r) Y_{l,m}{}^R(\vartheta,\varphi)$$

that is, employing the basis set χ_{ilm}

$$f = \Sigma_{ilm} \chi_{ilm} C_{ilm}$$

with

$$R_{lm}(r) = \Sigma_i \frac{1}{r} B_i(r) C_{ilm}.$$

Actually linear combination of spherical harmonics adapted to the full point group of the molecule are employed.[30]

In the Hamiltonian matrix, the kinetic energy and the nuclear attraction terms are easily calculated, whereas the electron−electron interaction is treated with a Kohn−Sham (KS) approach.[31] The Self-Consistent Field (SCF) electron density is obtained by a previous KS-LCAO calculation. The SCF density is then expanded on the OCE basis, then the Hartree potential is computed solving the Poisson equation. The exchange correlation potential is a function of the density and its gradient (LB94),[24] so it is calculated from the SCF density and expanded on the OCE basis.

The bound states are calculated by means of a generalized diagonalization of the KS Hamiltonian matrix H_{KS}, whereas the inverse iteration procedure[32] is employed to get the continuum

TABLE 1: Experimental and Calculated Valence Photoelectron Spectrum of Ferrocene

experiment [a]		LB94-GS (present results)		VWN-TS[b]	ADC(3)[c]
band	IP	MO	$-\epsilon$	$-\epsilon$	IP
A′	(6.86)[d]	$4e_2'$ (3d)	(9.48)[d]	(7.45)[d]	(7.85)[d]
	0.35	$8a_1'$ (3d)	0.23	0.19	1.51
A″	1.91	$6e_1'$ (π)	1.57	1.43	0.85
	2.42	$4e_1''$ (π+d)	2.27	2.03	1.23
B		$6a_2''$ (π)	4.20	3.96	5.72
B		$3e_2''$	4.29	4.17	5.11
B		$3e_2'$	4.40	4.22	5.23
B	5.34−6.44	$5e_1'$	4.77	4.68	6.04
B		$3e_1''$	5.11	5.08	6.22
B		$7a_1'$ (π)	5.37	5.43	5.86
C		$5a_2''$	7.93	7.74	9.54
C	9.74	$2e_2''$	8.25	8.08	10.07
C		$6a_1'$	8.27	8.18	9.95
C		$2e_2'$	8.45	8.36	10.37
D		$4e_1'$	12.45	12.63	
D		$2e_1''$	12.49	12.70	
E		$4a_2''$	16.55		
E		$5a_1'$	16.95		

[a] Ref 3. [b] Ref 11. [c] Ref 10. [d] Absolute energy for the first state. For all other states relative energies are reported. Values in eV.

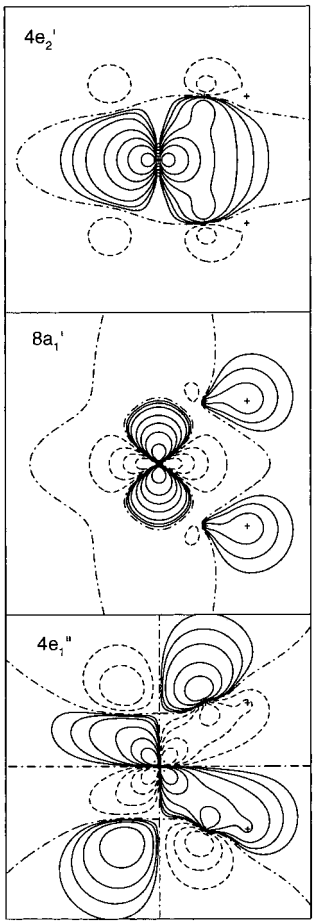

Figure 1. Contour plot relative to the $4e_2'$, $8a_1'$, and $4e_1''$ DZP eigenfunction of $Fe(Cp)_2$. Solid, dashed and dot−dashed lines correspond to positive, negative and zero contributions, respectively.

TABLE 2: Core Photoelectron Spectrum of Ferrocene

	LB94-GS		
BAND	MO	$-\epsilon$ (eV)	EXP IP (eV)
Fe 3p	$3e_1'$	60.17	66[a]
	$3a_2''$	61.44	
Fe 3s	$4a_1'$	92.32	
C 1s	[e]	290.67	290.03[b]
Fe 2p	$1e_1'$	711.55	715.8 [c]
	$1a_2''$	712.09	
Fe 2s	$2a_1'$	821.48	845[d]
Fe 1s	$1a_1'$	6997.58	7110[f]

[a] Ref 47. The value is referred to the experimental binding energy of the free atom. [b] Ref 39. [c] Ref 46. [d] Ref 45. [e] Complete list of the orbital is: $1e_2''$, $1e_2'$, $1e_1''$, $2e_1'$, $2a_2''$, $3a_1'$. [f] Ref 45.

states. The cross section and the asymmetry parameter are finally obtained via dipole transition moments and phase shifts.[19]

3. Computational Details

The SCF electron density is obtained from the LCAO-ADF program,[33,34] employing the LB94[24] exchange-correlation potentials and the STO DZP basis set taken from the optimized database included with the ADF package. The SCF procedure is performed with the GS configuration. The center of the OCE is set on the center of the molecule. The use of a very large basis set expansion of the effective potential and of the explicit continuum wave function allows to obtain results which are expected to be convergent in the chosen Hamiltonian. Present calculations are performed with a radial basis set of B-splines of order 10, defined over a radial grid consisting of 108 intervals, up to a radial cutoff $R_{max} = 20.022\,657$ au, and with the maximum angular momentum $L_{MAX} = 50$. This choice has been checked in a series of convergence tests performed on the photoionization profiles using different values of L_{MAX} (30, 50, and 60) and ensures that the reported profiles are convergent with respect to the OCE expansion.

The bound state calculations are performed on a workstation ALPHA 500 employing an iterative algorithm for the diagonalization, whereas the calculation of continuum states by inverse iteration procedure is performed with a parallel version of the program on a Cray T3E computer.

The experimental geometry[35] is employed in all calculations.

4. Results and Discussion

Photoelectron Spectrum. Before analyzing the continuum results, it is convenient to discuss the valence photoelectron spectrum obtained with the LB94-GS potential. It is well-known that the Kohn−Sham (KS) orbital formulation of the DFT together with the transition state (TS) approach, where the KS eigenvalue is optimized for a transition state with a fractional occupation number, provides a way to calculate the ionization potential with good accuracy. However, if the exact KS potential were employed, a theorem states that the first IP would equal the HOMO KS eigenvalue at the GS configuration.[36] Of course, the exact KS potential is not known, but the presently employed LB94 potential, having the correct asymptotic behavior, has shown very good agreement between the HOMO IP and the HOMO KS eigenvalue in atoms and small molecules.[24] Furthermore, good prediction of the IP over the complete energy range of the photoelectrum spectrum have been recently obtained

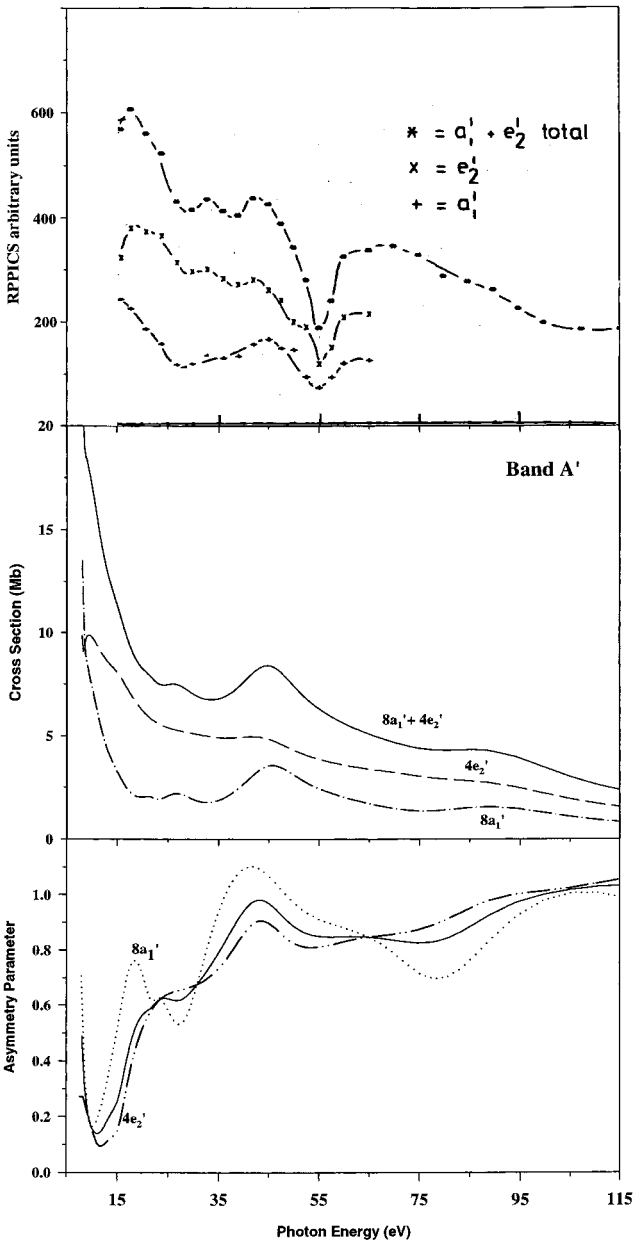

Figure 2. Calculated cross section (central panel) and asymmetry parameter profile (lower panel) of the Band A′ ($4e_2'$ and $8a_1'$ ionizations) of $Fe(Cp)_2$. Total asymmetry parameter: solid line. Experimental RPPICS values (upper panel) from ref 4. The calculated data are shifted to the experimental thresholds, ref 3.

for a series of molecules of various complexity,[25−27] so it is worth employing the LB94 eigenvalues calculated for the $Fe(C_5H_5)_2$ molecule in order to assign the calculated states to the observed experimental bands[3]. The results are reported in Table 1 together with the experimental data[3], the very recent theoretical IPs obtained with the DFT-TS approach by Plashkevych and co-workers,[11] very useful to test the reliability of the present LB94 eigenvalues, and the highest level ab initio results available in the literature.[10]

Looking at the data collected in Table 1, it is worth noting that the first absolute LB94-GS eigenvalue is strongly overestimated, whereas the energy shifts of the following states agree very well both with the experimental data and the VWN-TS results from ref..[11] We have also performed VWN-TS calculations of the valence ionization potentials, with the same STO-DZP basis set, which completely agree with the calculated IPs of ref 11. The ordering of the ionic states in Table 1 is the same

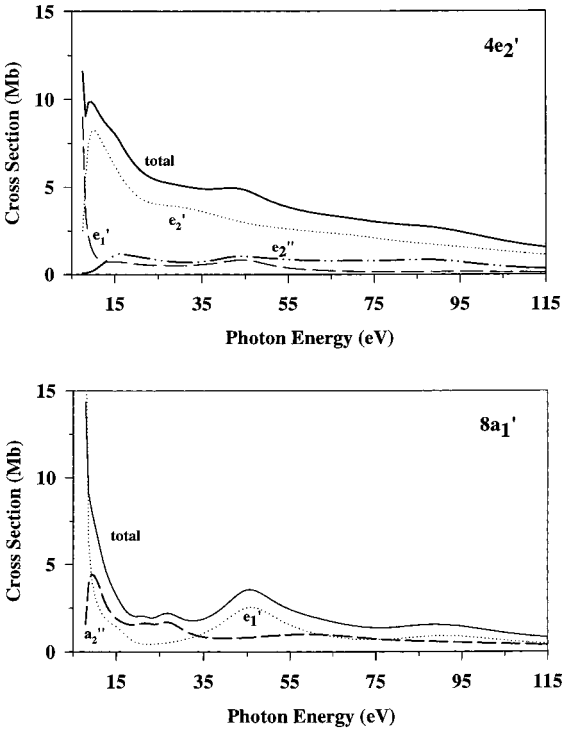

Figure 3. Partial final contributions to the $4e_2'$ and $8a_1'$ cross sections of $Fe(Cp)_2$. The calculated data are shifted to the experimental thresholds, ref 3.

in both calculations and correctly reproduces the experimental assignment relative to the first four ionizations. In any case, we believe that for the purposes of the present work, the correct ordering and energy separations of the orbitals are much more important than the agreement between the absolute energy values of the IPs, to associate the calculated states to the resolved photoelectron experimental bands and correctly sum up their cross section profiles to compare with the available cross section data.

To better discuss the present assignment of the PE spectrum, a brief recollection of the bonding in ferrocene can be useful. In the D_{5h} symmetry (with the two rings as is the gas phase), the π orbitals of the two $(C_5H_5)^-$ ligands yield three sets of orbitals: the low lying filled a_1' and a_2'' MOs, the set of filled e_1'' and e_1' MOs and a higher energy empty set of antibonding e_2' and e_2'' MOs. The 3d metal orbitals are split into three levels: a_1' (d_{z2}), e_2' (d_{x2-y2}, d_{xy}) both filled and e_1'' (d_{xz}, d_{yz}) unoccupied, which are of σ, δ, and π symmetry respectively with respect to the metal-ring axis. There is a strong bonding interaction between the e_1'' (π) ring orbital and the e_1'' (3d) metal orbital: therefore, the $4e_1''$ resulting MO has a mixed π ligand−3d metal character. The remaining 3d metal a_1' and e_2' orbitals give rise to essentially non bonding MOs ($8a_1'$ and $4e_2'$) with a largely 3d metal character. The experimental spectrum[3] shows four well-separated regions of ionizations, labeled A, B, C, and D (see Table 1). Region A contains two bands (A′ and A″) deriving from the highest occupied 3d metal and π ligand orbitals ($4e_2'$, $8a_1'$, $6e_1'$, and $4e_1''$), whose ordering is not definitely established, as already stressed. Region B is associated with the ionization from the remaining π ligand orbitals ($6a_2''$ and $7a_1'$) and the higher σ ligand MOs, whereas regions C and D are associated with the more strongly bound σ ligand MOs.

The present calculated spectrum (Table 1) is characterized by groups of closely spaced levels separated by a clear energy gap and reproduces correctly the experimental trend. As mentioned earlier, the most controversial issue is the energetic

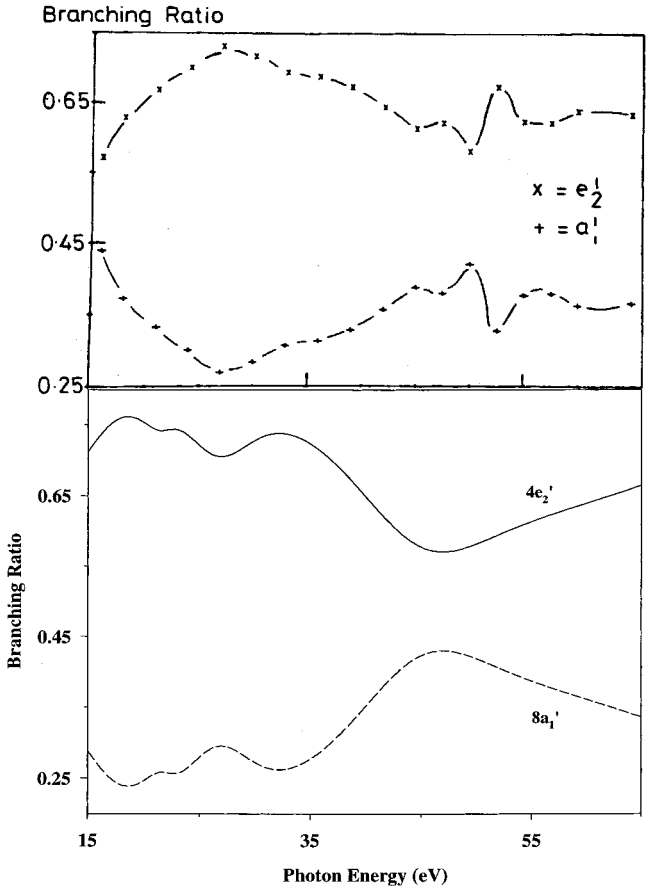

Figure 4. Experimental (upper panel), ref 4, and calculated (lower panel) branching ratio profiles of the $4e_2'$ and $8a_1'$ionizations (Band A′) of $Fe(Cp)_2$. The calculated data are shifted to the experimental thresholds, ref 3.

ordering of the highest four occupied molecular orbitals. The present theoretical results associate band A′ to the $4e_2'$and $8a_1'$ metal ionizations, whereas the next $6e_1'$ and $4e_1''$ ligand ionizations are relative to the two peaks of band A″, in line with the experimental indications.[3,4] The two highest occupied molecular orbitals ($4e_2'$and $8a_1'$) are calculated very close in energy, and their essentially 3d character is clearly manifest from Figure 1, where the isolines of the calculated relative eigenfuntions are plotted. It is interesting to observe, just at a qualitative level, that the $4e_2'$ eigenfunction also shows a small π ligand character, associated with the slight interaction between the e_2' 3d metal level and the higher energy empty e_2' π ring orbital, whereas the $8a_1'$ eigenfunction has a not negligible σ ligand participation, which could be responsible for the slightly lower energy presently found for this state with respect to the $4e_2'$ one. The $6e_1'$ and $4e_1''$ MOs are associated with π $C_5H_5^-$ ligand orbitals, as it is apparent also from Figure 1, although the $4e_1''$ eigenfunction also has a certain Fe 3d character (about 18%, according to the population analysis results).

The next group of calculated ionizations (from 4.20 to 5.37 eV of relative energy) are closely spaced and concerns the photoemission from $C_5H_5^-$ ligand orbitals. We propose to associate these levels ($6a_2''$, $3e_2''$, $3e_2'$, $5e_1'$, $3e_1''$ and $7a_1'$) to the experimental band B. In particular, the $6a_2''$ and $7a_1'$ levels (at 4.20 and 5.37 eV of relative energy) are associated with the two possible combinations of the lower energy orbitals of the two $(C_5H_5)^-$ fragments: the shift of more than one eV between these two levels reflects the presence of a direct interaction between the ligands through the π orbitals. (This has been drawn from the results of a simple LB94-GS calculation of the dimer

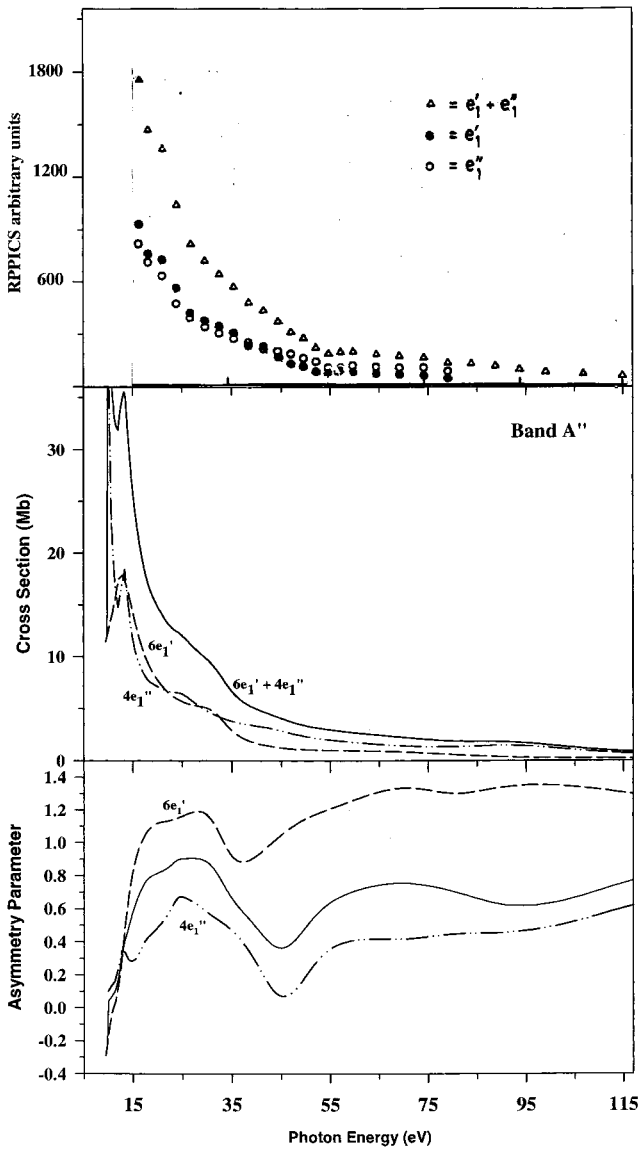

Figure 5. Calculated cross section (central panel) and asymmetry parameter profile (lower panel) of the Band A″ ($6e_1'$ and $4e_1''$ ionizations) of $Fe(Cp)_2$. Total asymmetry parameter:solid line. Experimental RPPICS values (upper panel) from ref 4. The calculated data are shifted to the experimental thresholds, ref 3.

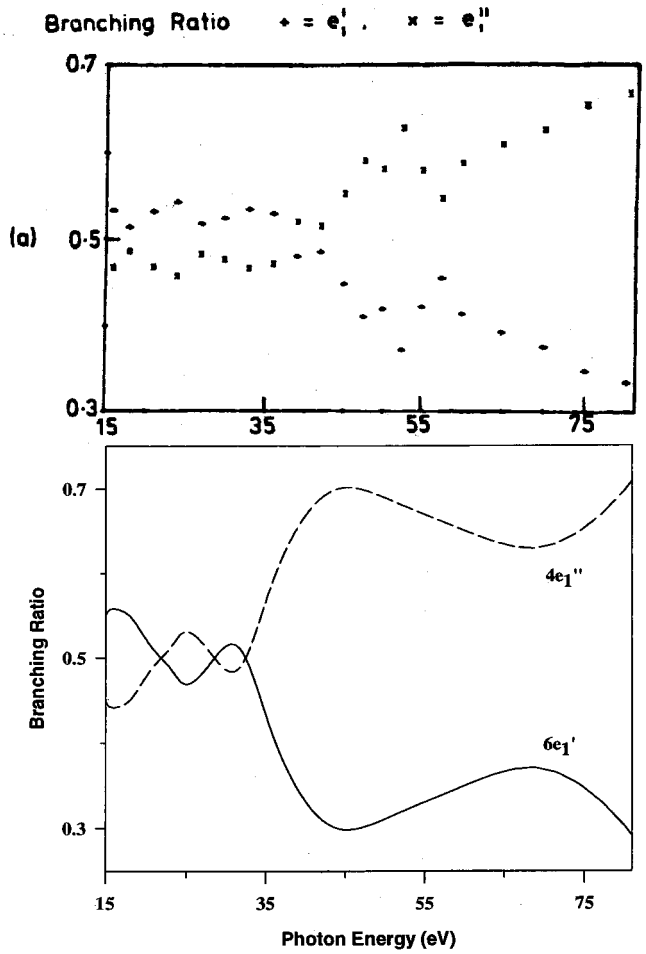

Figure 6. Experimental (upper panel), ref 4, and calculated (lower panel) branching ratio profiles of the $6e_1'$ and $4e_1''$ ionizations ′(Band A″) of $Fe(Cp)_2$. The calculated data are shifted to the experimental thresholds, ref 3.

$(C_5H_5^-)_2$). The remaining four ionizations contributing to band B are relative to the σ ring orbitals; the energy shift between the pairs of levels deriving from the same orbital of a $C_5H_5^-$ ring ($3e_2''$ and $3e_2'$; $5e_1'$ and $3e_1''$) is much smaller (only 0.1 and 0.4 eV) than that found for the π states, showing that the direct interaction between the σ ring orbitals is less effective along the molecular axis with respect to the π case. It is worth noting that a direct interaction between the $C_5H_5^-$ ligands is not surprising because their distance in $Fe(C_5H_5)_2$ is only 3.31 Å, even shorter than the distance between the carbon planes in graphite (3.35 Å)).

The following group of four closely calculated ionizations (from 7.93 to 8.45 eV of relative energy) contributes to band C, which appears therefore well separated by the previous band B, in nice accord with the experiment. These levels are associated with the $5a_2''$, $2e_2''$, $6a_1'$ and $2e_2'$ σ ring initial states. The inner valence D and E bands have not yet experimentally studied; the D band is visible only in the He(II) experimental spectrum and appears well separated from the lower energy C band[3]. The present theory predicts a gap of about 4 eV between these bands. Almost the same energy gap separates also the D and E calculated bands and both of them are contributed by a pairs of levels ($4e_1'$, $2e_1''$ and $4a_2''$, $5a_1'$ respectively) deriving from the ionization of the inner ring orbitals. The calculated LB94-GS core binding energies are reported in Table 2 for completeness.

Valence Photoionization Profiles. The calculated cross section and asymmetry parameter profiles of the band A′ ($4e_2'$ and $8a_1'$ orbitals) are reported in Figure 2 together with the experimental RPPICS (Relative Partial Photoionization Cross Section) from ref 4, useful for a direct comparison. The theoretical total cross section exhibits a steep decrease after the threshold followed by small maxima. A first weak maximum is visible around 25 eV photon energy, whereas a more pronounced feature is present around 45 eV. Eventually, a very weak and broad feature lies at higher energy (around 90 eV). The examination of the separate cross section of the $4e_2'$ and $8a_1'$ ionizations contributing to band A′ reveals that the maxima in the total profile are essentially associated with the $8a_1'$ ionization, whereas the $4e_2'$ cross section shows a monotonic decrease with photon energy, apart from a weak increase just around 45 eV, much less pronounced than that in the case of the $8a_1'$ profile. The e_2' band appears always more intense than the $8a_1'$ band, apart from a narrow energy region just above the threshold. The different behavior of the ionization continua of two essentially 3d metal MOs can be related to the different ionization channels available for the e_2' and a_1' ionizations (ke_1',

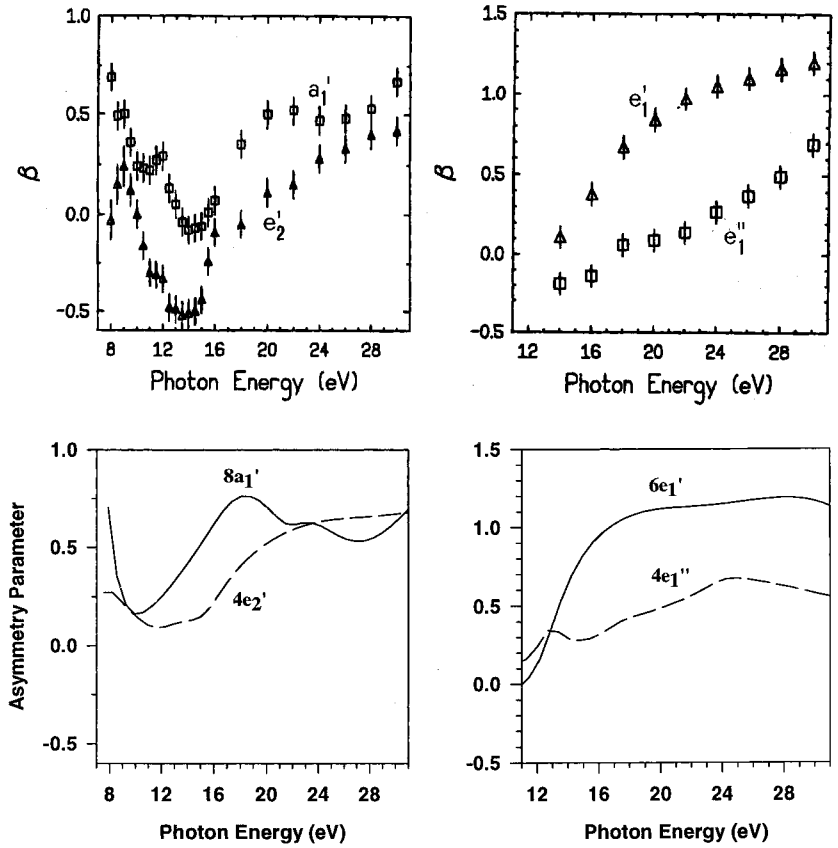

Figure 7. Calculated (lower panels) and experimental (upper panels), ref 5, asymmetry parameter profiles for the Fe 3d $8a_1'$ and $4e_2'$ orbitals and for the π ligand $6e_1'$ and $4e_1''$ orbitals of $Fe(Cp)_2$. The calculated data are shifted to the experimental thresholds, ref 3.

ke_2' and ke_2'' for e_2' electrons and ka_2'' and ke_1' continua for a_1' electrons) and their relative contributions to the final continuum wave functions, as it is shown in detail in Figure 3. It is well apparent that the $4e_2'$ cross section is dominated by the final ke_2' continuum contribution in all energy range, whereas the ke_1' continuum gives the most important contribution to the intensity of the $8a_1'$ ionization, in particular in the energy region around 40 eV. The analysis of the partial continuum contributions allows therefore to associate the shape resonance calculated around 45 eV to the $8a_1' \rightarrow ke_1'$ transition; all the other continuum channels essentially contribute to the background of the cross section. To verify if this shape resonance could be associated with a virtual valence state, we have performed a minimal basis set calculation whose results do not indicate however any eigenvalue higher than 14 eV. Therefore, this higher energy feature cannot be explained with this simple model. As concerns the comparison with the experimental data (see Figure 2), it is apparent the lack in the calculated profiles of the strong minimum present both in the partial and total experimental profiles around 55 eV. This sharp structure has been previously attributed to resonant photoemission of 3d electrons in the vicinity of 3p−3d giant resonant absorption, a kind of process that the present level of the theory cannot describe. The absence of such structures in the calculated profiles can be an indirect evidence of the experimental assignment to an autoionization. This multielectron processes can be treated by the Time Dependent extension of the present theory (TD-DFT), as it has been recently shown in the case of atoms[37] and small molecules,[38] but at the moment, the TD-DF code is still impracticable for larger systems. Apart from the minimum, the other experimental features of the band A′ profile are correctly described by the theory. In particular a good accord is found for the energy position of the quite pronounced maximum observed around 42 eV in the experiment and calculated around 45 eV, as previously discussed. Also, the relative intensities of the $4e_2'$ and $8a_1'$ profiles are correctly reproduced by the calculations, with the $4e_2'$ cross section always more intense than the $8a_1'$ one. It is interesting to underline that a similar behavior has been found also in the calculated 3d metal band cross sections of $Cr(C_6H_6)_2$[27], where the $8a_{1g}$ (HOMO) profile (band A) displays a large shape resonance around 40 eV, whereas the $4e_{2g}$ one (band B) decreases over the whole energy range. The nature of the initial states is the same in the two organometallic compounds with the a_{1g} and a_1' levels corresponding to the $3d_{z2}$ metal MO and the e_{2g} and e_2' levels representing the d_{x2-y2}, d_{xy} metal MO, in $Cr(C_6H_6)_2$ and $Fe(C_5H_5)_2$ molecules, respectively. In this respect therefore, the behavior of the cross section profile could be used as a fingerprint of the symmetry of the 3d metal initial state. The different behavior of the 3d metal ionization continua is associated with the different final channels available for the relative ionizations, in line with a previous hypothesis.[4]

The Figure 4 compares the experimental and calculated branching ratios of the $4e_2'$ and $8a_1'$ ionizations. Also, in these curves, the agreement between theory and experiment is very satisfactory: the experimental profiles again highlight the difference in cross section behavior between the $4e_2'$ and $8a_1'$ bands with a larger cross section of $4e_2'$ band in all energy range. More important, significant deviations are observed from the statistical ratio 2:1 due to orbital occupancies, which are followed very well by the calculated profiles, with the exception of the near threshold region. A change in the slope is observed just before the region of the autoionization. The behavior of the calculated curves is the same although the slope change is

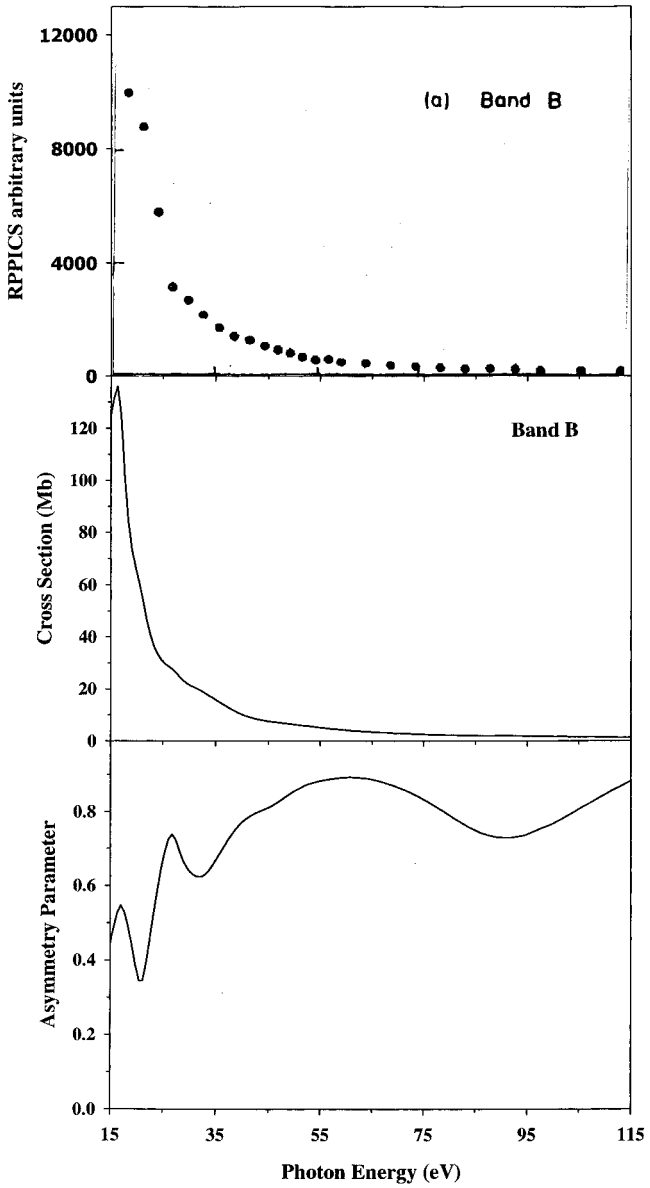

Figure 8. Calculated cross section (central panel) and asymmetry parameter profile (lower panel) of the Band B of $Fe(Cp)_2$. Experimental RPPICS values (upper panel) from ref 4. The calculated data are shifted to the experimental threshold value 12.75 eV, ref 3.

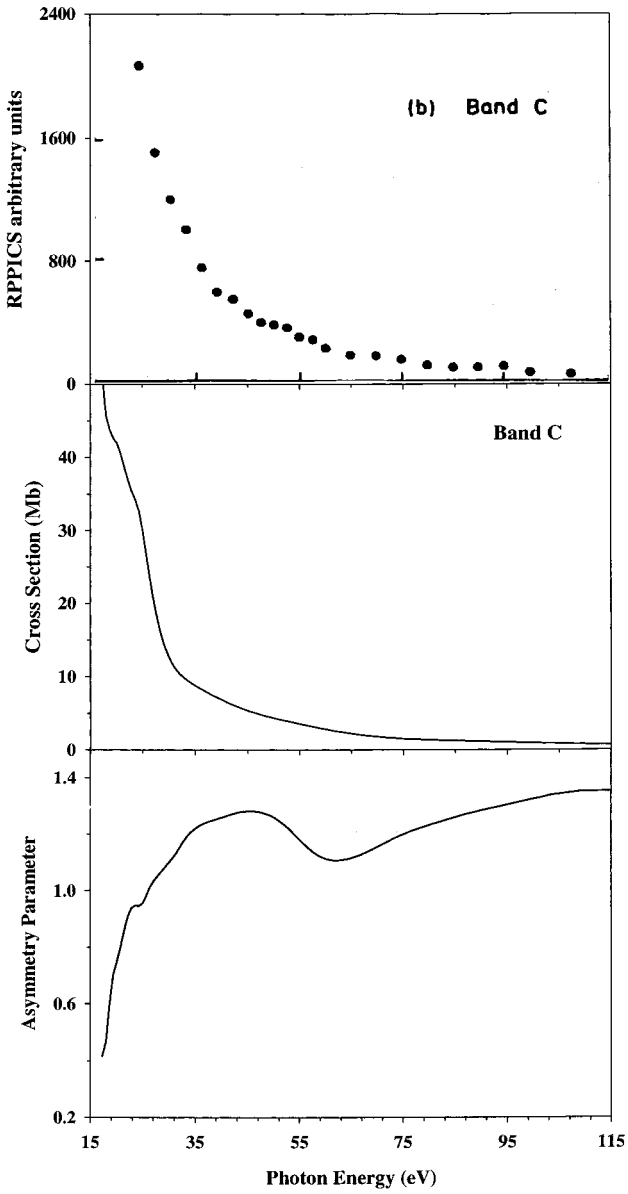

Figure 9. Calculated cross section (central panel) and asymmetry parameter profile (lower panel) of the Band C of $Fe(Cp)_2$. Experimental RPPICS values (upper panel) from ref 4. The calculated data are shifted to the experimental threshold value 16.60 eV, ref 3.

somehow more pronounced for the lack of the autoionization structures in the theoretical profiles.

Consider now the results for the band A″ of ferrocene which is assigned to the $6e_1'$ and $4e_1''$ ligand ionizations. The calculated cross sections of the two MOs and of their sum are reported in Figure 5, together with the experimental data.[4] The $6e_1'$ and $4e_1''$ theoretical profiles show a quite different behavior at the threshold, with the $4e_1''$ cross section much more intense than the $6e_1'$ one, whereas around 14 eV a shape resonance can be identified in both profiles. This structure is also present in the lower energy total cross section. Above 15 eV the two partial and the total cross sections show a similar monotonic decrease with photon energy; this behavior reproduces correctly the trend observed for the experimental data (upper panel) and in particular the relative intensities of the partial and the total profiles. The narrow resonances calculated just above the threshold are not present in the measure.

A closer inspection of the behavior of the $6e_1'$ and $4e_1''$ bands is possible through the branching ratios plots presented in Figure 6, where the experimental and theoretical data are compared. The agreement between theory and experiment[4] is nice. The calculated curves correctly display the change of the oscillation amplitude observed around 45 eV, although they appear slightly shifted toward lower energy with respect to the experiment. This discrepancy can be related to the quite attractive character of the LB94-GS potential which generally lowers the calculated energies of the cross section profiles with respect to the results obtainable with the VWN-TS potential. Again, it is remarkable the strong deviation from the 1:1 statistical ratio, as well as the out of phase oscillations in the two cross sections at low energy, both well reproduced by the calculations, so that the assignment would be completely definite of this basis alone. In fact, the experimental branching ratio behavior has allowed to assign the two measured cross sections to the $4e_2''$ and $6e_1'$ ionizations, as reported in Figure 6. In particular the lower intensity observed for the e_1'' band at low energy and its increase in the region around 45 eV has been considered as an evidence of a partial 3d metal character of the orbital ionized.[4] The theoretical results

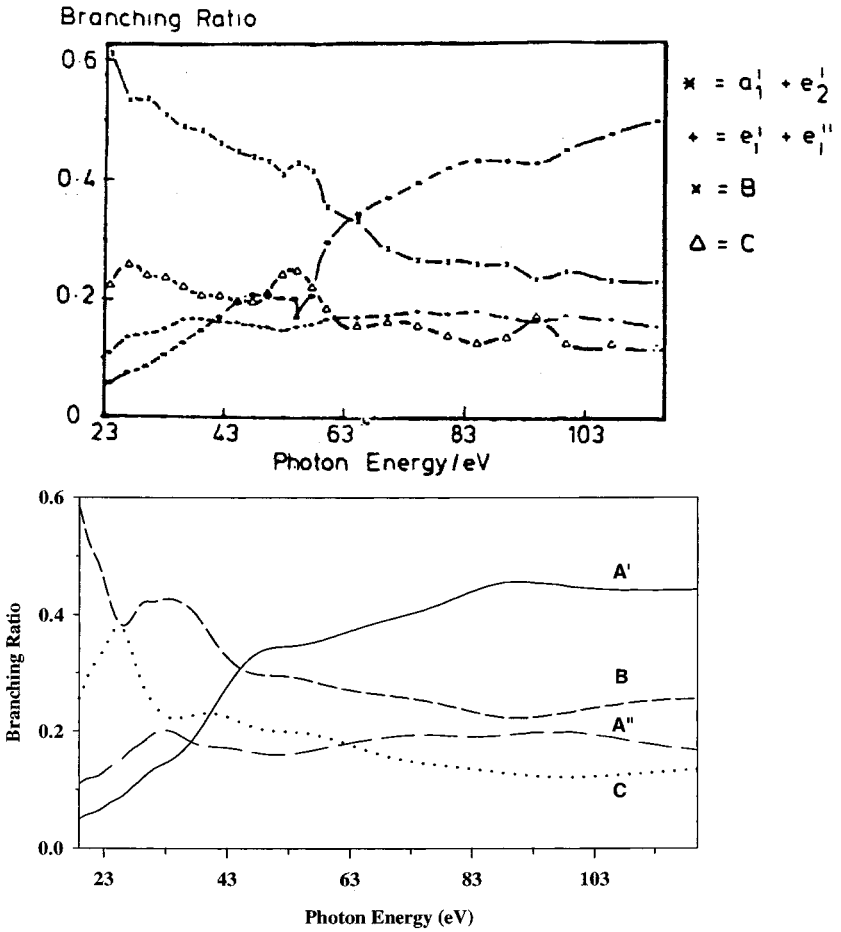

Figure 10. Experimental (upper panel) [4] and calculated (lower panel) valence-band branching ratios of $Fe(Cp)_2$. The calculated data are shifted to the experimental thresholds, ref 3.

confirm the experimental attribution; however, in addition to the composition of the initial states the different intensity observed for the $4e_1''/6e_1'$ branching ratio can also be related to the symmetry properties of the initial state and the consequent different ionization channels available for the continuum states.

In summary the present results for the A′ and A″ bands of the PE spectrum of ferrocene indicate that the initial states of mainly 3d metal or ligand character can be clearly distinguished by their cross section behavior. These findings confirm the qualitative deduction drawn from the trends experimentally observed and point out in particular that the information content of the calculated cross section data in organometallic compounds is such as to provide strong support to the interpretation of PE spectra, in terms of the symmetry and AO composition of the relevant orbitals.

The calculated asymmetry parameter profiles of the bands A′ and A″ are reported in Figures 2 and 5, respectively. The A′ band β profile appears quite structured in the lower energy range and it is possible to identify clearly the counterparts of the structures also found in the total cross section of the band A′, in particular a minimum near the threshold and the maximum around 45 eV. At higher energy, only very smooth features are present. The asymmetry parameter profile of band A" (Figure 5) shows a rapid increase just above the threshold again resembling the trend followed by the calculated cross section profile. A definite minimum is instead present around 45 eV. The lower energy part of the calculated asymmetry parameter profiles can be compared with the experimental data available[5] in Figure 7. Here, the β profiles of the single MOs contributing to the A′ and A″ bands are shown. The minimum in the experimental profile of the $8a_1'$ and $4e_2'$ 3d Fe MOs is well apparent around 14 eV, which is well reproduced by the calculation. The experimental data relative to the ligand MOs show instead a monotonic increase in this energy range, as correctly predicted also by the theory. Also, the relative trends of the calculated profiles of the two couple of MOs in each band follow the observed curves and can confirm the experimental attribution of the initial states. The present results suggest therefore that possible relationships can be found between the asymmetry parameter profiles and the metal or ligand character of the ionized orbitals and underline also the interest to extend the experimental measure toward higher energies where stronger resonance in the 3d metal cross sections are present.

Cross sections and asymmetry parameter profiles calculated for bands B and C are reported in Figures 8 and 9 together with the experimental data from Ref 4. These bands are associated with the lower π and the first σ ligand ionizations (see Table 1). As it is well apparent in the two figures, the cross section profiles of both B and C bands exhibit a monotonic decrease with photon energy with only one significant difference at threshold where the intensity of B band is stronger than that of C band, due to the larger number of ionizations contributing to it. The theoretical results reproduce correctly the experimental behavior in all energy range and confirm the common trend followed by the cross sections of the $C_5H_5^-$ ligand ionizations bands in ferrocene.

The calculated asymmetry parameter of B band (Figure 8) shows some oscillations at low energies while very smooth structures are present in the β profile above 40 eV. The asymmetry parameter of the C band (Figure 9) appears less

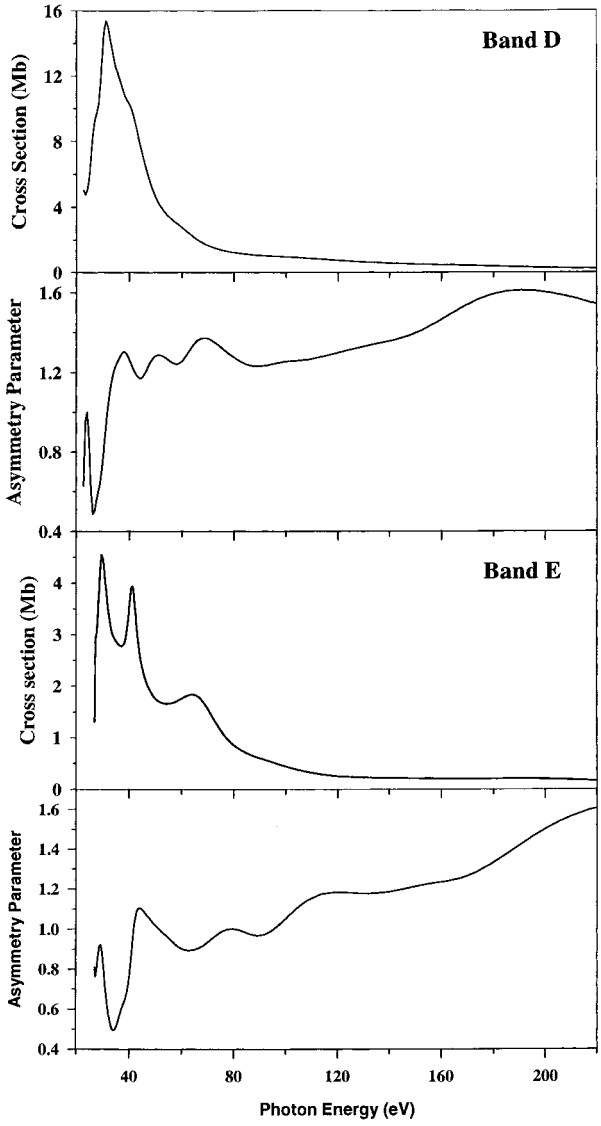

Figure 11. Calculated cross sections and asymmetry parameter profiles of the D and E inner valence Bands of $Fe(Cp)_2$.

structured with a monotonic increase from the threshold up to 45 eV.

A last comparison between experimental and theoretical results relative to the valence ionizations is reported in Figure 10, where the branching ratios of the A′, A″, B, and C bands are shown. Again, the overall agreement of the theoretical curves with the experimental ones is excellent and is clearly able to discriminate without ambiguity between different bands, although at low energy some discrepancies are apparent, namely a too high calculated profile for the C band with respect to the B band.

The last inner valence ring ionizations give rise to the D and E bands (see Table 1) whose calculated results are reported in Figure 11. No experimental data are available for comparison. The cross section of band D presents a maximum around 40 eV followed by a rapid decline with photon energy. The asymmetry parameter profile appears quite structured up to 80 eV, whereas at higher energy, the behavior is rather smooth and without structures. The next band E displays two important structures near the threshold and a weaker feature around 65 eV. It appears that quite typical pattern are calculated for the inner valence bands at variance with the behaviors of the profiles of the outer valence ligand bands. The structures present in the asymmetry parameter profile of band E extend in the same energy range of the corresponding ones in the cross section. It is important to underscore that the features present in the asymmetry parameter profiles of all the ligand valence bands are strong enough to be experimentally detected and often fall in an energy region where the cross section profile is already very weak.

Core Photoionization Profiles. Consider first the core results relative to the C 1s profiles which are collected in Figure 12. The experimental continuum resonances derived from electron energy loss spectrum[39] are also reported for comparison. The theoretical C 1s cross section has been obtained as the sum of the partial contributions of each core C 1s orbital ($1e_2''$, $1e_2'$, $1e_1''$, $2e_1'$, $2a_2''$, $3a_1'$, see also Table 2). Two near, well-resolved peaks are present just above the ionization threshold (at 295 and 298 eV respectively) showing a pattern very similar to that calculated also in the C 1s continuum spectrum of $Cr(C_6H_6)_2$ and free C_6H_6[27], and found in the C 1s spectra of other six-electrons aromatics,[40,41] where two continuum resonances are also observed. In the case of the $Fe(C_5H_5)_2$ molecule the inspection of the calculated partial final channel cross section profiles contributing to all the C 1s initial states allow to attribute the two peaks calculated just above the C 1s ionization threshold as follows: both maxima mainly derive from the $1e_1''$ and $2e_1'$ initial orbitals; the other C 1s initial states contribute only to the background of the total C 1s cross section in this energy region. The first peak (at 295 eV) can be attributed to the $2e_1' \rightarrow ka_2'$ and $1e_1'' \rightarrow ka_1''$ transitions, whereas the second one (at 298 eV) to the $2e_1' \rightarrow ke_2'$ and $1e_1'' \rightarrow ke_2''$ transitions (the other possible final channels allowed for these two initial orbitals give only minor contributions to these two peaks). On the basis of a minimal basis set (MBS) calculation, performed with the LB94-GS potential, we can found the eigenvalues of the quasi bound virtual valence states of interest: $1a_2'$ 9.18 eV and $1a_1''$ 9.21 eV; $7e_2'$ 11.53 eV and $6e_2''$ 11.56 eV. These values appear realistic, apart from the slight overestimate of the absolute energies: in fact, the energy shift between $1a_2'$, $1a_1''$ and $7e_2'$, $6e_2''$ final virtual orbitals is about 2.4 eV from the MBS calculation and 3 eV from the continuum calculation. It has also to be underlined that these four MBS virtual states have an essentially Carbon 2p character. In summary, we can conclude that the two C 1s continuum peaks in $Fe(C_5H_5)_2$ can be interpreted as shape resonances determined by cyclopentadienyl rings in analogy with the interpretation given for the similar structures in the C 1s cross section of $Cr(C_6H_6)_2$.[27] Actually, the only significant difference near the threshold between the two organometallic compounds is a shift of the energy position of the two maxima, which are calculated at higher photon energy for $Cr(C_6H_6)_2$ (at 297.2 and 299.9 eV respectively) with respect to $Fe(C_5H_5)_2$. Being the shift in the C 1s experimental thresholds very small (290.03 eV in $Fe(C_5H_5)_2$ and 289.7 eV in $Cr(C_6H_6)_2$) this effect is therefore due to the continuum, which shifts the profiles depending on the effective molecular potential.

The reliability of the present C 1s theoretical results is supported by the comparison with the experimental data available in the energy region just above the threshold (panel b of Figure 12). As we can see, the agreement with the experiment is very nice, in particular as concerns the energy position; also, the relative intensities of the two continuum shape resonances are well-described. The region at higher energy presents two smooth structures around 330 and 360 eV, which cannot be related to any virtual valence states due to their very high energy positions. In summary, the comparison between the $Fe(C_5H_5)_2$

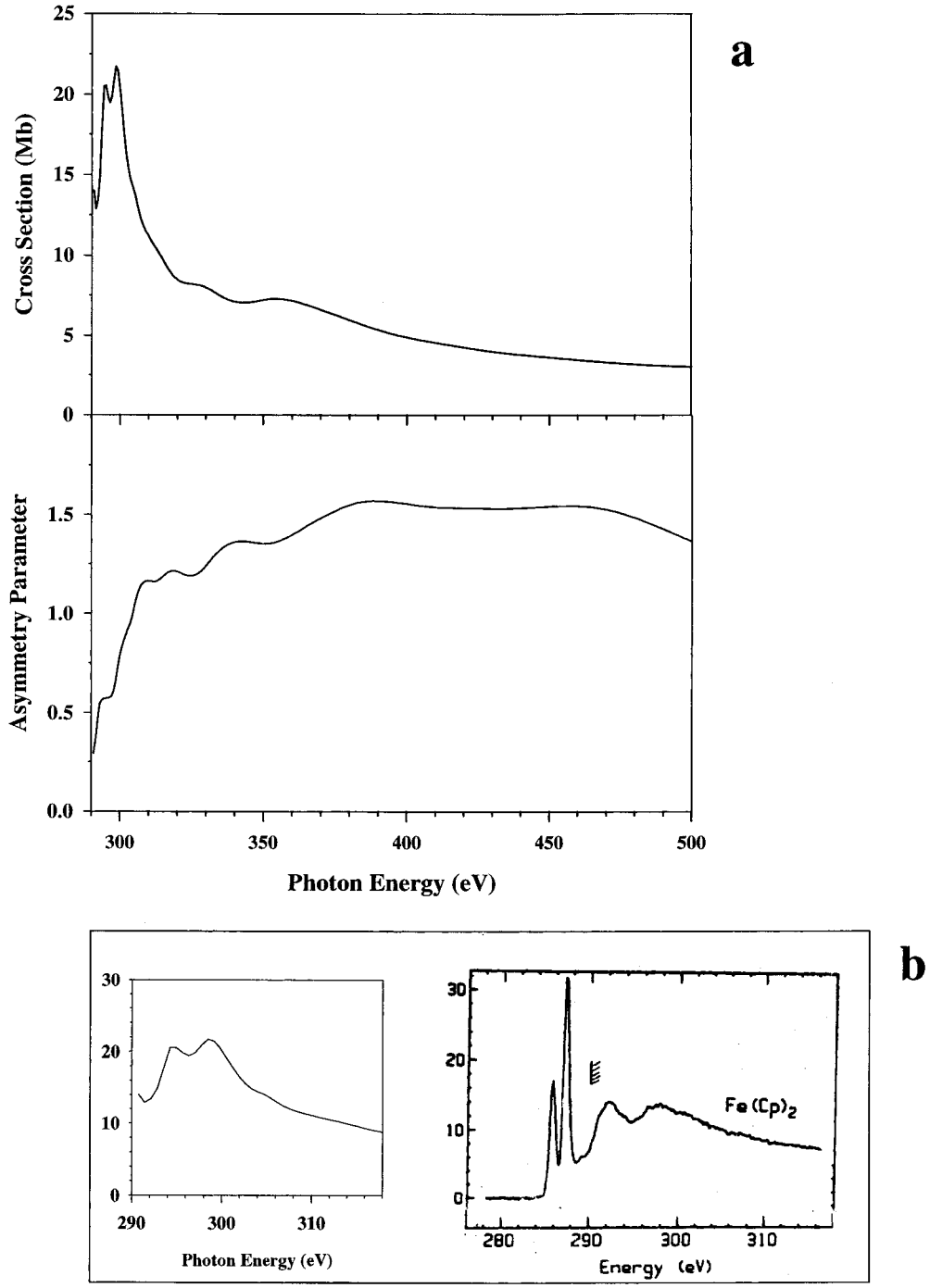

Figure 12. Calculated core C 1s cross section and asymmetry parameter profile (panel **a**) of $Fe(Cp)_2$. Comparison between calculated cross section and experimental ISEELS spectrum from ref 39 in the lower energy range (panel **b**). The calculated data are shifted to the experimental C 1s threshold, ref 44.

and $Cr(C_6H_6)_2$ results suggests that the behavior of the C 1s cross section near the threshold is determined essentially by the ligand fragments, with very small effect due to the coordination with the metal atom. This can be associated with the similarity of the initial states with the C 1s character in the two kind of ligands ($C_5H_5^-$ and C_6H_6) and to the fact that at low photon energies the continuum states do not penetrate into the system and feel essentially the potential of the ligand fragments.

The C 1s asymmetry parameter profile (Figure 12) does not show important features; a regular increase characterizes the region above the threshold, whereas at higher energies a quite constant trend is apparent.

Consider now the results relative to the metal core Fe 1s ionization, which are reported in Figure 13, together with the experimental XANES spectrum from ref 42. The calculated Fe 1s cross section profile shows a strong resonance at threshold characterized by a shoulder on the low energy side and followed by a series of broad and smooth oscillations. The lower energy part of the calculated spectrum is in good accord with the experimental XANES spectrum[42], as it is shown in panel b of Figure 13. An important observation is that the weak feature labeled D in the experiment is not reproduced by the calculation. This "bump" has been previously assigned to a multielectron shake-up satellite,[42] which cannot be described by the present level of theory. The shoulder B and the main structure C are

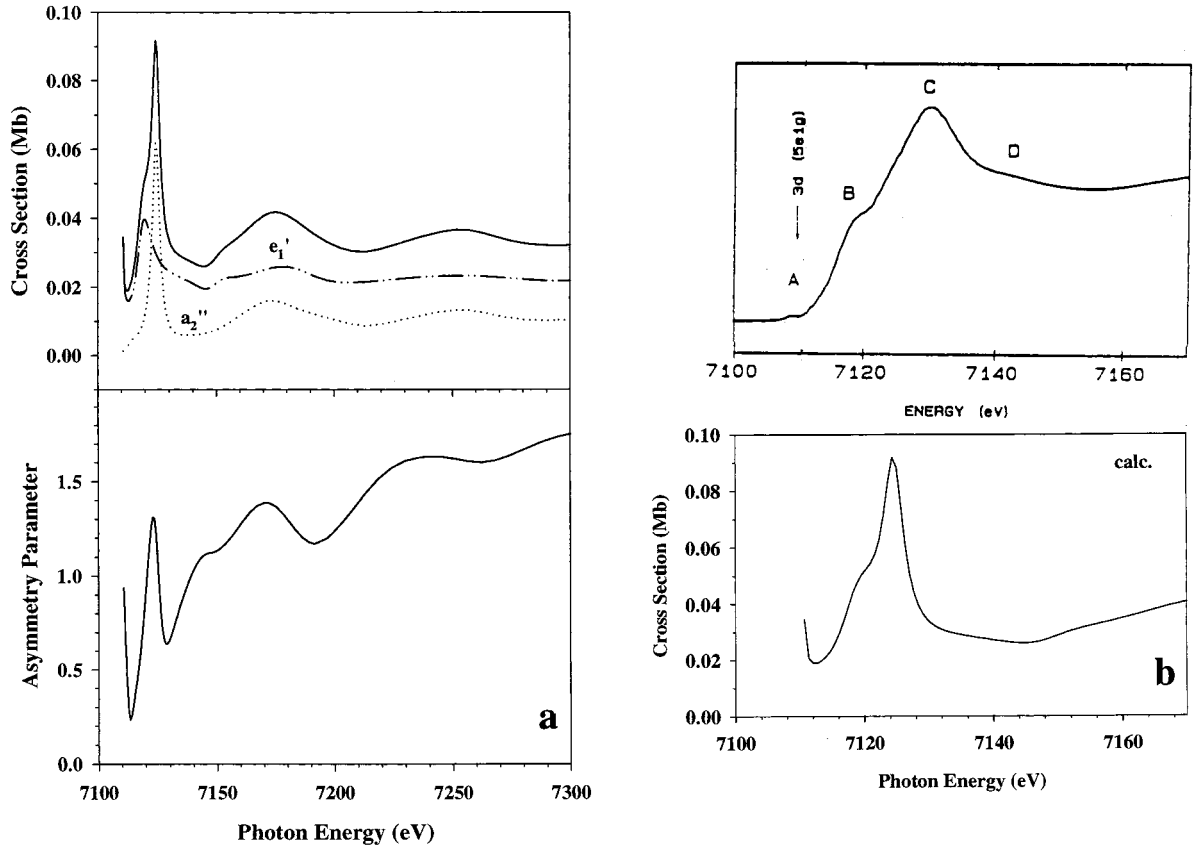

Figure 13. Calculated core Fe1s cross section and asymmetry parameter profile (panel **a**) of $Fe(Cp)_2$. Partial final continuum contributions (ke_1' and ka_2'')are also reported. Comparison between experimental XANES spectrum from ref 42 and calculated cross section in the lower energy range (panel b**).** The calculated data are shifted to the experimental Fe1s threshold, ref 45.

instead well-reproduced in the calculated spectrum and are associated with a shape resonance contributed by two components, as it is apparent from panel a, where the partial continuum contributions to the cross section are also shown. These are associated with p-like electron waves, namely ka_2'' and ke_1' channels, which gain their oscillator strength from the atomic s → p nature of the transitions. In particular, the lower energy shoulder derives from the $1a_1' \rightarrow ke_1'$ transition, whereas the main peak is associated with the $1a_1' \rightarrow ka_2''$ transition. The calculated energy splitting between these two continuum components (ka_2'' corresponds to the p_z electron wave and ke_1' to the p_x, p_y waves) is 4.8 eV. It is interesting to note that this value is higher than that found in the calculated Cr 1s cross section of $Cr(C_6H_6)_2$,[27] which closely resembles the present Fe1s profile, apart from a less pronounced lower energy shoulder of the shape resonance at threshold, due to the smallest splitting of the p waves (3.4 eV). The higher energy part of the Fe 1s profile shows a series of oscillations which can be the first terms of EXAFS oscillations. Also, this part of the spectrum is very similar to the Cr 1s profile in $Cr(C_6H_6)_2$. The comparison between the metal 1s continuum results of $Fe(C_5H_5)_2$ and $Cr(C_6H_6)_2$ seems to indicate that the spectra are not influenced by the change of the central metal atom if the nature of the ligands in the metal complexes remains substantially the same.

The Fe 1s asymmetry parameter profile (Figure 13) is very structured, at variance with the behavior observed for the C 1s results, in particular at the threshold where a significant correspondence with the structures in the cross section is apparent. Also at higher energies rather wide structures are present.

The results relative to the Fe 2s and 3s ionizations are not reported because they are essentially the same as those of Fe 1s, with only the exception of the absolute cross section values, which differ by a factor of about 4 and 8 respectively with respect to the Fe 1s values.

In Figure 14 the Fe 2p core ionization is considered; the $1a_2''$ and $1e_1'$ contributions relative to the splitting of the 2p orbitals in the D_{5h} symmetry are also reported. Several structures are present in the cross section profiles: a narrow peak just above the threshold (at 719.29 eV), a second more intense and large peak (around 740 eV) and a third less intense structure (around 792 eV), which is the first of a series of damped oscillations. The analysis of the initial partial contributions shows that the first resonance derives its intensity essentially from the $1e_1'$ initial state while the second and third structures are actually the sum of the $1e_1'$ and $1a_2''$ initial contributions. A more detailed interpretation requires the analysis also of the partial final continuum contribution accessible from each initial state. On ionization from metal 2p orbitals we expect d-like electron waves to dominate the cross section, namely ka_1' (d_{z2} wave), ke_1'' (d_{xz}, d_{yz} waves) and ke_2' (d_{x2-y2}, d_{xy} waves) channels; both the $1e_1'$ and $1a_2$" initial states have access to the a_1' and e_1'' ionization channels. The calculations show that the ke_2' continuum is the most responsible for the intensity of the first peak while both the ke_2' and ke_1'' channels are involved in the strongest resonance around 740 eV and in the first oscillation at 792 eV. The dominant contribution is always associated with the ke_2' continuum. The a_1' continuum carries only minor intensity increasing substantially the background of the cross section profile. A close resemblance of the calculated Fe 2p cross section profile with the Cr 2p continuum results in $Cr(C_6H_6)_2$ molecule[27] is apparent, as found also for the metal 1s ionizations results. In summary, the core continuum spectra of these two organometallic compounds, which share ligands

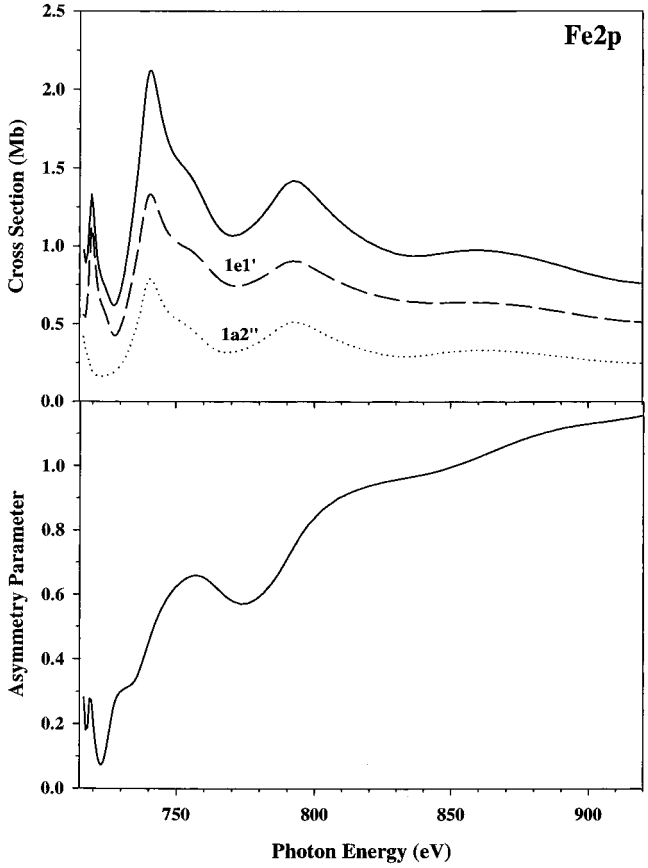

Figure 14. Calculated core Fe 2p cross section and asymmetry parameter profile of $Fe(Cp)_2$. Initial orbital contributions ($1e_1'$ and $1a_2''$) are also reported. The calculated data are shifted to the experimental Fe 2p threshold, ref 46.

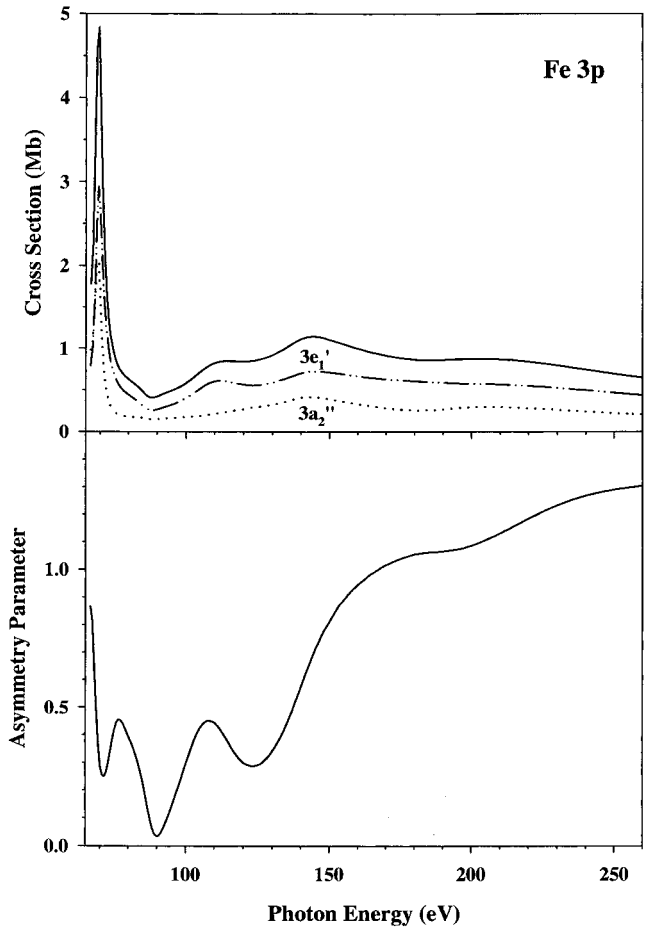

Figure 15. Calculated core Fe3p cross section and asymmetry parameter profile of $Fe(Cp)_2$. Initial orbital contributions ($3e_1'$ and $3a_2''$) are also reported. The calculated data are shifted to the Fe3p free atom experimental threshold, ref 47.

of similar nature, exhibit very similar behavior and no obvious dependence on the central metal atom is apparent. As concerns the comparison with experimental data, the only available spectrum at our knowledge is relative to a EELS measurement (around the Fe 2p ionization thresholds) of Hitchcock et al.[43] However, apart from further difficulties due to the presence of the preedge L_3 and L_2 spin−orbit components, the measured oscillator strength for the below edge absorptions is much higher than the calculated absolute cross section values (almost 1 order of magnitude). Therefore, the continuum resonances are hidden in the background of the experimental spectrum. Higher resolution photoabsorption measurements could probably reveal also the continuum resonance present between the two Fe 2p ionization thresholds and few tens of eV above the L_2 edge.

Consider finally the Fe 3p ionization, whose results are collected in Figure 15. The 3p orbital is not properly a core orbital, however its energy (around 60 eV) is well separated from the valence shell energies so that it can be discussed together with the other core orbitals. The strong difference of the Fe 3p profile with respect to the Fe 2p one is immediately apparent, at variance with the situation found for the core metal ns ionizations. The cross section is dominated by a very sharp and intense peak near the threshold followed by a minimum (at 88.4 eV) which can be associated with a Cooper minimum because the 3p wave function has a radial node. This is an atomic effect, and in fact a minimum at 83.8 eV has been calculated for free Fe atom, using the LB94 potential. At higher energies only smooth oscillations are present in the cross section. The initial partial contribution reported in the upper panel show that both the $3e_1'$ and $3a_2''$ initial states contribute to the intensity of the strong peak at the threshold. The analysis of the partial final contributions indicates instead that the intensity derives from the ka_1' continuum channel both for the two initial states, at variance with the Fe 2p ionization where this channel gives only minor contribution. This final state could correspond both to d-like or s-like electron waves. We could rationalize this result considering the simple model of the minimal basis set calculations; in this way, we can identify the first virtual valence level of a_1' symmetry above the threshold as a quasi-bound state involved in the resonance. This is the $9a_1'$ level whose composition shows a strong Fe 4s character and a smallest 3d one. It is probable however that the Fe 3d contribution carries most of the intensity of the resonance because the 3p−4d atomic transition is more intense than the 3p−4s one. Also, the Fe3p cross section profile looks very similar to that calculated for the Cr3p ionization in $Cr(C_6H_6)_2$.[27]

The asymmetry parameter profile (Figure 15) appears very structured at low energy and in particular shows a strongly decrease toward zero at the Cooper minimum with rapid variations in the vicinity of this minimum, as expected in the atomic species.

Conclusions

The continuum photoionization observables of ferrocene, cross section, branching ratios, and asymmetry parameter profiles have been calculated and analyzed in detail, exploring the complete energy range from valence to metal core ionizations.

The valence photoelectron spectrum obtained with the LB94-GS potential is in good accord with the experiment both as concerns the energetic ordering and the spacing among the observed ionizations. This has allowed to associate the calculated states to the resolved experimental bands and sum up correctly their cross section profiles. The outer valence cross section profiles and branching ratios have been compared with the experimental data showing a good agreement between theory and experiment. This indicates the capability of the computational method employed to deal with large system containing transition metal atom. Most important, the level of agreement between theory and experiment is such as to discriminate very clearly between cross sections and angular distributions due to different initial orbitals, so that the LDA description presently adopted appears generally adequate to give a detailed interpretation of photoemission data in organometallic compounds and to resolve assignment problems in the spectra.

The calculated shape resonances have been analyzed in terms of both the initial and final states contributing to them, adding new information generally not obtainable from the experimental data. Several comparison with analogous results obtained for the $Cr(C_6H_6)_2$ molecule are made, to highlight possible relationships in the cross section profiles. The theoretical results indicate that the initial states of mainly 3d metal and mainly ligand character can be clearly distinguished by their cross section behavior and point out the important information content which can be drawn from this continuum observable. As concerns the asymmetry parameter profiles, the calculations indicate the presence of important structures in the valence region, even at high energies, which could be experimentally detected.

The core C 1s features near to the threshold are interpreted as shape resonances to quasi-bound valence virtual orbitals of the cyclopentadienyl ring in line with the interpretation given also for the analogous structures in the C 1s cross section of $Cr(C_6H_6)_2$. The metal core cross sections (Fe 1s, 2p, and 3p) display in general very sharp structures at threshold followed by broad oscillations and show strong similarity with the cross section profiles calculated for the same Cr core ionizations in $Cr(C_6H_6)_2$. Apparently, the cross section behavior of the core metal orbitals does not seem influenced by the change of the central metal atom in these two organometallic compounds. It is expected a stronger sensitivity of the metal core results in response to a different chemical environment of the central atom.

Acknowledgment. This work has been supported by grants from MURST of Italy. A generous INSTM grant of computer time on the CRAY T3E of CINECA (Bologna) is gratefully acknowledged.

References and Notes

(1) Evans, S.; Green, M. L. H.; Jewitt, B.; Orchard, A. F.; Pygall, G. F. *J. Chem. Soc. Faraday II* **1972**, *68*, 1847.
(2) Rabalais, J. W.; Werme, L. O.; Bergmark, T.; Karlsson, L.; Hussain, M.; Siegbahn, K. *J. Chem. Phys.* **1972**, *57*, 1185.
(3) Cauletti, C.; Green, J. C.; Kelly, M. R.; Powell, P.; Van Tilborg, J.; Robbins, J.; Smart, J. *J. Electron Spectrosc. Relat. Phenom.* **1980**, *19*, 327.
(4) Cooper, G.; Green, J. C.; Payne, M. P. *Mol. Phys.* **1988**, *63*, 1031.
(5) von Wald, G. A.; Taylor, J. W. *J. Electron Spectrosc. Relat. Phenom.* **1988**, *47*, 315.
(6) Coutiere, M.; Demuynck, J.; Veillard, A. *Theor. Chim. Acta* **1972**, *27*, 281.
(7) Baerends, E. J.; Ros, P. Chem. Phys. Lett. **1973**, *27*, 39.
(8) Rösch, N.; Johnson, K. H. Chem. Phys. Lett. **1974**, *24*, 179.
(9) Bagus, P. S.; Walgren, U. I.; Almlöf, J. *J. Chem. Phys.* **1976**, *64*, 2324.
(10) Ohno, M.; Von Niessen, W.; Schüle, J. Chem. Phys. **1991**, *158*, 1.
(11) Plashkeych, O.; Ågren, H.; Karlsson, L.; Pettersson, L. G. M.; J. Electron Spectrosc. Relat. Phenom. **2000**, *106*, 51.
(12) Davies, C. E.; Green, J. C.; Kaltsoyannis, N.; MacDonald, M. A.; Qin, J.; Rauchfuss, T. B.; Refern, C. M.; Stringer, G. H.; Woolhouse, M. G. *Inorg. Chem.* **1992**, *31*, 3779 and ref. therein.
(13) Green, J. C.; *Acc. Chem. Res.* **1994**, *27*, 131.
(14) Venuti, M.; Stener, M.; Decleva, P. *Chem. Phys.* **1998**, *234*, 95.
(15) Stener, M.; Decleva, P. *J. Electron Spectrosc. Relat. Phenom*. **1999**, *104*, 135.
(16) Venuti, M.; Stener, M.; De Alti, G.; Decleva, P. *J. Chem. Phys.* **1999**, *111*, 4589.
(17) Stener, M.; Fronzoni, G.; Venuti, M.; Decleva, P. *Chem. Phys. Lett.* **1999**, *309*, 129.
(18) Dill, D.; Dehmer, J. L. *J. Chem. Phys.* **1974**, *61*, 692.
(19) Dill, D.; Dehmer, J. L. In *Electron−Molecule and Photon-Molecule Collisions*; Rescigno, T., McKoy, V., Schneider, B., Eds.; Plenum: New York, 1979, p 225.
(20) Yang, D. S. Bancroft, G. M.; Puddenphatt, R. J.; Tan, K. H.; Cutler, J. N.; Bozek, J. D. *Inorg. Chem.* **1990**, *29*, 4956.
(21) Bursten, B. E.; Green, J. C.; Kaltsoyannis, N.; MacDonald, M. A.; Sze, K. H.; Tse, J. S. *Inorg. Chem.* **1994**, *33*, 5086.
(22) Xiarong Li, Bancroft, G. M.; Puddephatt, R. J.; Liu, Z. F.; Hu, Y. F.; Tan, K. H. *J. Am. Chem. Soc.* **1994**, *116*, 9543.
(23) Xiarong Li, Tse, J. S.; Bancroft, G. M.; Puddephatt, R. J.; Tan, K. H. *Organometallics* **1995**, *14*, 4513.
(24) Van Leeuwen, R.; Baerends, E. J. *Phys. Rev. A* **1994**, *49*, 2421.
(25) Stener, M.; Furlan, S.; Decleva, P. *J. Phys. B* **2000**, *33*, 1081.
(26) Stener, M.; Furlan, S.; Decleva, P. *Phys. Chem. Chem. Phys*. **2001**, *3*, 19.
(27) Stener, M.; Fronzoni, G.; Furlan, S.; Decleva, P. *J. Chem. Phys.* **2001**, *114*, 306.
(28) Vosko, S. H.; Wilk, L.; Nusair, M. Can. J. Phys. **1980**, *58*, 1200.
(29) de Boor, C. *A Practical Guide to Splines*; Springer: Berlin, 1978.
(30) Burke, P. G.; Chandra, N.; Gianturco, F. A. J. Phys. B **1972**, *5*, 2212.
(31) Parr, R. G.; Yang, W. *Density Functional Theory of Atoms and Molecules*; Oxford University Press: New York, 1989.
(32) Brosolo, M.; Decleva, P. *Chem. Phys.* **1992**, *159*, 185.
(33) Baerends, E. J.; Ellis, D. E.; Ros, P. *Chem. Phys.* **1973**, *2*, 41.
(34) Fonseca Guerra, C.; Snijders, J. G.; te Velde, G.; Baerends, E. J. *Theor. Chem. Acc.* **1998**, *99*, 391.
(35) Bohn, R. K.; Haaland, A. *J. Organometallics Chem.* **1966**, *5*, 470.
(36) Levy, M.; Perdew, J. P.; Sahni, V. *Phys. Rev. A* **1984**, *30*, 2745.
(37) Stener, M.; Decleva, P.; Lisini, A. *J. Phys. B* **1995**, *28*, 4973.
(38) Stener, M.; Decleva, P. *J. Chem. Phys.* **2000**, *112*, 10 871.
(39) Rühl, E.; Hitchcock, A. P. *J. Am. Chem. Soc.* **1989**, *111*, 5069.
(40) Doering, J. P.; Gedanken, A.; Hitchcock, A. P.; Fischer, P.; Moore, J.; Olthoff, J. K.; Tossell, J.; Raghavachari, K.; Robin, M. B. *J. Am. Chem. Soc.* **1986**, *108*, 3602.
(41) Newbury, D. C.; Ishii, I.; Hitchcock, A. P. *Can. J. Chem.* **1986**, *64*, 1145.
(42) Ruiz-Lopez, M. F.; Loos, M.; Goulon, J.; Benfatto, M.; Natoli, C. R. *Chem. Phys.* **1988**, *121*, 419.
(43) Hitchcock, A. P.; Wen, A. T.; Rühl, E. *Chem. Phys.* **1990**, *47*, 51.
(44) Bakke, A. A.; Jolly, W. L.; Schaaf, T. F. J. *Electron Spectrosc. Relat. Phenom.* **1977**, *111*, 339.
(45) Hitchcock, A. P.; Mancini, D. C. *J. Electron Spectrosc. Relat. Phenom.* **1994**, *67*, 1.
(46) Jolly, W. L. Bomben, K. D.; Eyermann, C. J. *At. Data Nucl. Data Tables* **1984**, *31*, 433.
(47) Shirley, D. A.; Martin, R. L.; Kowalczyk, S. P.; McFeely, F. R.; Ley, L. *Phys. Rev. A* **1977**, *15*, 544.